On the Optimal Azimuth Offset for Individual Pitch Control in Aeroelastic Code Coupled with a High-Fidelity Flow Solver

Van Vondelen, A. A.W.; Pamososuryo, A. K.; Navalkar, S. T.; Van Wingerden, J. W.

DOI
10.23919/ECC64448.2024.10590980

Publication date
2024

Document Version
Final published version

Published in
Proceedings of the European Control Conference, ECC 2024

2024 European Control Conference (ECC)
June 25-28, 2024. Stockholm, Sweden

On the Optimal Azimuth Offset for Individual Pitch Control in Aeroelastic Code Coupled with a High-Fidelity Flow Solver

A.A.W. van Vondelen[1], A.K. Pamososuryo[1] S.T. Navalkar[2], and J.W. van Wingerden[1]

Abstract— **To justify the use of two single-input single-output (SISO) control loops instead of more complex multi-input multi-output (MIMO) control, the axes in a wind turbine's pitch control system should be fully decoupled using the multi-blade coordinate transform. To achieve that, usually, an azimuth offset is required, correcting for phase lags originating from, e.g., actuator delays and blade flexibility. In wind turbine simulations, this parameter is commonly obtained by analysis of the linearized turbine models. This work, however, demonstrates that analyzing linearized turbine models is not sufficient for correcting the full phase lag when coupling wind turbine simulation tools to large-eddy simulators (LES), since additional phase lags may arise. Instead, this work proposes deriving the azimuth offset using data-driven modelling directly in coupled LES, where data is generated by exciting the structure with pseudo-random binary noise. Using this approach it was found that the optimal azimuth offset is three degrees higher than when using the linearized model, which demonstrates that deriving the optimal azimuth offset from linearized models is not suitable for coupled simulations.**

I. INTRODUCTION

Over the past decades, wind turbines have experienced significant growth with a visible trend for offshore installations [1]. Building bigger turbines pays off since doubling rotor diameter theoretically quadruples the power capacity of the machine thanks to their quadratic relation [2]. However, a considerable challenge comes with larger rotors, namely the increasing asymmetric loads, arising from the spatiotemporal variability in the wind, such as turbulence, wind shear, tower shadow, yaw misalignment, and wake overlap imposed by upstream turbines [3]. As a blade slices through the varying wind field at the rotor frequency (once-per-revolution/1P), the blade fatigue damage is exacerbated at this frequency and its harmonics (2P, 3P, etc.), whereas the fixed structure experiences that of 0P, 3P, 6P, etc. for a three-bladed wind turbine. Such loading accelerates the degradation of a turbine's structural integrity, thereby shortening its lifetime. Although structural reinforcements can be done, these might be cost-prohibitive, which motivates the resort to control solutions, such as individual pitch control (IPC).

Conventional IPC relies on the blade moments projection from the rotating frame into the tilt and yaw axes in the fixed frame, accomplished by the azimuth-dependent multi-blade coordinate (MBC) transformation [3]. Therein, a diagonal single-input single-output (SISO) control structure could be designed, assuming that the two control channels are fully decoupled. The resulting control inputs are then projected back by the inverse transformation, yielding individual pitch signals counteracting the 1P loading. In reality, however, the decoupled channel assumption does not always hold, for instance, due to pitch actuator delays and/or blade flexibility. As a remedy, an azimuth offset is required in the MBC transformation, whose optimal value can decouple both channels, thereby justifying simple SISO control designs, and preventing degradation of the load control performance [4], [5]. Mulders et al. [4] provide a comprehensive study on this offset, including derivation of its analytical expression. They have shown the existence of a sensitivity peak surrounding the 1P frequency, which may amplify unwanted frequencies surrounding the 1P frequency if not corrected by the azimuth offset.

For determining such an optimal offset, a system model is commonly available, e.g., through the linearization routine of mid-fidelity wind turbine simulation tools based on the blade-element momentum (BEM) theory. One example of such a tool is the National Renewable Energy Laboratory's (NREL) OpenFAST [6]. Nevertheless, for wind farm wake and wake interaction studies, these simulators need to be coupled with high-fidelity large-eddy-simulator (LES) tools, such as AMR-Wind [7]. This enables the computation of more complex wind flow structures not only for more reliable advanced controller validation and load analysis but also for optimization of wind farm layout design, turbulence effects investigation, and study of the overall performance and efficiency of wind energy systems.

The LES codes, however, commonly utilize actuator line or disk methods [8] for their aerodynamic solvers and are run at much lower simulation frequency than the wind turbine simulation tools due to the high computational expense. Thus, to make coupled simulations computationally feasible, they are often run by substepping[1] the wind turbine simulator with respect to the LES code and interpolating the data points [9]. However, the discrepancies between these coupled tools might invalidate the optimal azimuth offset found solely on the linearized model, as some degree of coupling between the control axes may remain.

Since the azimuth offset may be sensitive to the above uncertainties, it can be argued that identifying a model in the coupled LES and wind turbine simulator code is more straightforward, and reduces the analyst's need to identify

[1]A.A.W. van Vondelen, A.K. Pamososuryo, and J.W. van Wingerden are with the Delft Center for Systems and Control, Delft University of Technology, 2628 CD Delft, The Netherlands {A.A.W.vanVondelen, A.K.Pamososuryo, J.W.vanWingerden}@tudelft.nl

[2]S.T. Navalkar is with Siemens Gamesa Renewable Energy B.V., Prinses Beatrixlaan 800, 2595 BN The Hague, The Netherlands Sachin.Navalkar@siemensgamesa.com

[1]That is, both software are run at different timescales.

the required compensation for the introduced phase lags in the coupled simulation. The main contribution of this paper is hence threefold:

- Demonstration of the discrepancy between the optimal azimuth offset derived from linearized models and the actual optimal azimuth offset in coupled LES simulations.
- Provision of a data-driven modelling framework for deriving the optimal azimuth offset in coupled LES simulations.
- Quantification of the optimal azimuth offset in a coupled LES simulation for the International Energy Agency (IEA) 15-MW reference wind turbine [10].

The remainder of this paper is organized as follows. The next section introduces the methodology used in this study, including descriptions of the control system, simulation setup, and system identification procedures. Section III presents the results obtained from the system identification, and analyzes these results by subjecting them to various metrics. In Section IV, conclusions are drawn and a recommendation is provided for robust azimuth offset quantification.

II. METHODOLOGY

This section introduces the methodology used in this study. First, a brief overview of the conventional IPC with the azimuth offset inclusion is given, after which the simulation setup is presented. Following, the system identification framework is described, including the quantification procedure of the optimal azimuth offset using the relative gain array.

A. Conventional IPC with Azimuth Offset

A conventional IPC makes use of the individual blade root bending moments measured by strain gauges in the rotating reference frame. These moments are then mapped into the fixed frame, resulting in the orthogonal collective, tilt, and yaw axes/channels, by the forward MBC transformation T_{MBC} as follows

$$\begin{bmatrix} M_{\text{col}} \\ M_{\text{tilt}} \\ M_{\text{yaw}} \end{bmatrix} = \underbrace{\frac{2}{3}\begin{bmatrix} 1/2 & 1/2 & 1/2 \\ \cos(\psi_1) & \cos(\psi_2) & \cos(\psi_3) \\ \sin(\psi_1) & \sin(\psi_2) & \sin(\psi_3) \end{bmatrix}}_{T_{\text{MBC}}(\psi)} \begin{bmatrix} M_1 \\ M_2 \\ M_3 \end{bmatrix}, \quad (1)$$

for a three-bladed wind turbine, as considered in this work. In (1), the notation M_i represents the i-th blade root bending moment, where $i \in \{1,2,3\}$, M_{col}, M_{tilt}, and M_{yaw} denote the collective, tilt, and yaw moments. The i-th blade azimuth is denoted $\psi_i = \psi + 2(i-1)\pi/3$, in which $\psi = \int \omega_{\text{r}}\,\text{d}t$ is the first blade's azimuth with ω_{r} as the rotor frequency (1P) and where t represents time. Note that, as the M_{col} is unused for the IPC design, this component is dropped from the following derivations.

The 1P component in the blade load is now mapped as DC components in the tilt and yaw axes and is subject to cancellation by the controller. This is done by a pair of identical SISO compensators, e.g., integrators, assuming that these channels are decoupled. In the frequency domain, this is represented as follows

$$\begin{bmatrix} \beta_{\text{tilt}}(s) \\ \beta_{\text{yaw}}(s) \end{bmatrix} = \begin{bmatrix} C(s) & 0 \\ 0 & C(s) \end{bmatrix} \begin{bmatrix} M_{\text{tilt}}(s) \\ M_{\text{yaw}}(s) \end{bmatrix}, \quad (2)$$

where $C(s) = k/s$, in which s denotes the Laplace variable. The constant gain k is chosen depending on the desired controller bandwidth.

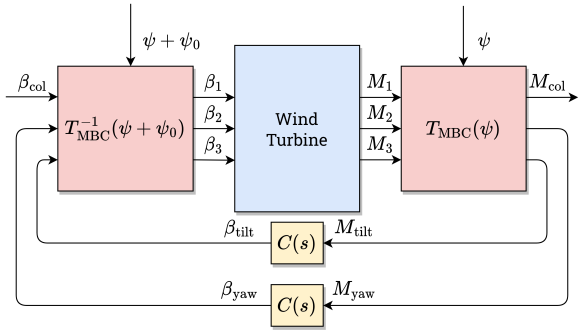

Fig. 1. Schematic of the conventional individual pitch controller with azimuth offset.

The exerted tilt and yaw pitch control actions, β_{tilt} and β_{yaw}, respectively, can then easily be translated to their rotating frame representation using the inverse MBC transformation

$$\begin{bmatrix} \beta_1 \\ \beta_2 \\ \beta_3 \end{bmatrix} = \underbrace{\begin{bmatrix} 1 & \cos(\psi_1+\psi_0) & \sin(\psi_1+\psi_0) \\ 1 & \cos(\psi_2+\psi_0) & \sin(\psi_2+\psi_0) \\ 1 & \cos(\psi_3+\psi_0) & \sin(\psi_3+\psi_0) \end{bmatrix}}_{T^{-1}_{\text{MBC}}(\psi+\psi_0)} \begin{bmatrix} \beta_{\text{col}} \\ \beta_{\text{tilt}} \\ \beta_{\text{yaw}} \end{bmatrix}, \quad (3)$$

with the collective pitch contribution β_{col} provided externally. The notation β_i represents the individual blade pitch angle. The inverse transformation T^{-1}_{MBC} also includes the azimuth offset ψ_0, the optimal value of which decouples the tilt and yaw channels and justifies the SISO control design in (2) [4]. A schematic overview of the conventional IPC controller is given in Fig. 1. Note that for simplicity, pitch actuator dynamics are neglected in this paper. Nevertheless, tilt-yaw cross-coupling may still exist, for instance, due to blade dynamics.

B. Simulation setup

In this work, a toolchain of NREL codes is used. First, the considered turbine is the IEA 15-MW reference fixed-bottom offshore wind turbine [10], of which relevant parameters are highlighted in Table I. Second, the turbine is simulated in OpenFAST, a well-established mid-fidelity wind turbine simulation tool, which can be run standalone with a BEM aerodynamics module, or coupled, as in our case, to LES, such as AMR-Wind. AMR-Wind relies on the AMReX framework, which features block-structured adaptive mesh refinement and efficient parallelism techniques [11].

The turbine is controlled using the reference open-source controller (ROSCO) [12]. This controller leverages modern control features such as a wind speed estimator, tip speed

TABLE I

KEY PARAMETERS OF THE IEA 15 MW.

Parameter	Value	Unit
Rated power	15	MW
Hub height	150	m
Rotor diameter	240	m
Cut-in wind speed	3	m/s
Cut-out wind speed	25	m/s
Rated wind speed	10.59	m/s
Min. rotor speed	5	rpm
Max. rotor speed	7.56	rpm

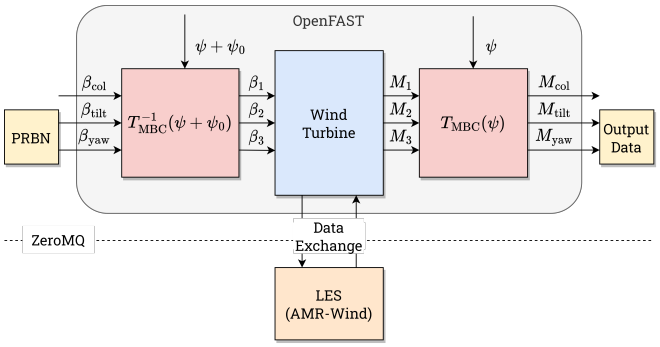

Fig. 2. Schematic of the system identification setup, including the coupling of the individual pitch controller in OpenFAST with AMR-Wind.

ratio tracking controller, and 1P and 2P IPCs. Besides these modules, ROSCO allows overriding the control setpoints with user-defined setpoints, which can be communicated through a protocol known as ZeroMQ [13]. By parsing messages and effectively bypassing the baseline pitch controller, the setpoints can more easily be generated in a higher-level scripting language, such as Python. From this environment, it is straightforward to generate a pseudo-random binary noise (PRBN) excitation signal and feed it to the pitch actuators.

Simulations are carried out in a coupled OpenFAST AMR-Wind environment. Earlier work that employed this coupling approach can be found in the work of Taschner et al. [14]. OpenFAST operates with a time step of 0.005 seconds, while AMR-Wind simulates the free stream flow using a 10 times larger time step of 0.05 seconds. Data exchange between AMR-Wind and OpenFAST is achieved through interpolation and leverages an actuator line model [15].

In the current investigation, laminar inflow conditions are employed to ensure precise system identification around the desired operating point of 9 m/s. The simulation extends over a duration of 1500 seconds, where the initial 250 seconds of simulation are discarded to account for startup effects.

The computational domain measures 4160 meters in the x-direction, 3200 meters in the y-direction, and 1600 meters in the z-direction. The wind turbine is located at coordinates ($x = 1200$ meters, $y = 1600$ meters). Throughout the domain, a spatial discretization of 10 meters is applied. However, within a smaller region starting 4.5 times the rotor diameter away before the turbine, a higher spatial resolution of 5 meters is utilized. This region has dimensions ($x = 3840$ meters, $y = 960$ meters, $z = 600$ meters).

C. Data-driven modelling

The OpenFAST linearized model is obtained by following the procedure described in [16]. IPC, as mentioned in Section II-A, operates in the azimuth-independent fixed frame. To obtain a model in that reference frame, a total of 36 models are obtained by linearizing the nonlinear equations as soon as the turbine reaches a periodic steady state after start-up. Consequently, these models represent the turbine dynamics at a different azimuthal position in the rotating frame, spaced equally by 10 degrees. Upon transforming these using the MBC transform and subsequently averaging them, the azimuthal dependence is removed and the model covers the linear dynamics averaged across the full rotor disk in the turbine's fixed coordinate frame around the desired operating point. Although matrix averaging is performed, as recommended in [16], other more suitable averaging approaches may provide better results, as shown in [17].

Black box system identification in the coupled OpenFAST AMR-Wind environment is performed using a method called optimized predictor-based subspace identification ($\text{PBSID}_{\text{opt}}$) [18], a variation of the well-known stochastic subspace identification method (see e.g. [19] for an overview of subspace identification methods). This method relies on input/output data for identification, which is obtained by exciting the system with a sufficiently persistently exciting excitation signal, usually composed of a noise sequence covering a broad spectrum of frequencies.

Using both identification approaches, a linear-time invariant model is obtained, which, generally, for nonlinear systems such as wind turbines, is only valid for a limited operating range. If IPC is desired for a range of wind speeds, the models and their optimal azimuth offsets must be determined for each case separately.

The system is excited and measured in the fixed coordinate frame, which heavily simplifies the identification process. As an excitation signal, PRBN is chosen. This signal is preferred because its amplitude can be constrained, unlike with random noise. The frequency content of the excitation signal is limited to 8 Hz, covering the full actuator bandwidth and sufficiently exciting the relevant dynamics. A schematic overview of the identification setup is given in Fig. 2.

Once a system is identified, the degree of coupling can be studied by analyzing the relative gain array (RGA) (see, e.g., [20]), which indicates the relative gain between inputs and outputs:

$$\text{RGA}(A) \triangleq A \odot (A^{\dagger})^{T}, \tag{4}$$

where $A \in \mathbb{R}^{l \times n}$ is the frequency response function of the system; $\odot$ denotes the element-wise multiplication, and $\dagger$ denotes the pseudo-inverse. The RGA is usually computed as a function of frequency and then averaged to obtain a single matrix. In our case, we compute the RGA between 0.1 and 1 rad/s.

Since the objective is system decoupling, the gain between the tilt command and tilt moment should approach 1, whereas the gain between the tilt command and yaw moment should

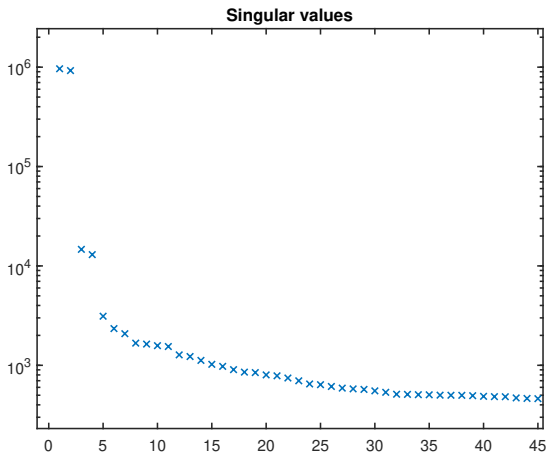

Fig. 3. Singular value plot of the first 45 singular values.

approach 0, and vice-versa. In other words, the RGA should approach identity I. By incrementing a phase offset in the inverse MBC transformation (3), the RGA should approach I, upon which the optimal azimuth offset can be selected.

III. RESULTS

After introducing the framework in the previous section, this section discusses the results obtained after applying the framework to the IEA 15-MW in AMR-Wind coupled with OpenFAST. First, the system identification results are discussed in detail, and several metrics are presented which are used to analyse the identification performance. Second, the optimal azimuth estimation is done on the identified model by analysing the RGA, upon which the found optimal azimuth offset is compared against the azimuth offset obtained from linearized models using the sensitivity function.

A. System identification

As a preprocessing step for model identification using $\text{PBSID}_{\text{opt}}$, singular values can be extracted from the input/output data (for details regarding this step, see [21]). By assessing their magnitudes, one can intuitively decide which to include. Opting for a too-high order might lead to overfitting, while selecting a too-low order may exclude important dynamics. Typically, this process is tackled iteratively.

The singular value plot resulting from the obtained input/output data for identification is shown in Fig. 3. Only the first 45 singular values are included in this figure, which is more than sufficient for identification. An immediate starting point for selecting the identification order is order 2, which includes the two largest singular values. Increasing the order beyond 11 will most likely not improve the identification results as the differences between the singular values become negligible.

Upon selecting orders 2 until 11, the identification is performed, which yields a state-space representation. The validity of this model can be further assessed by comparison with the linearized model from OpenFAST and a spectral average of the input-output data for the frequency range of interest. Figure 4 shows the Bode plots of the diagonal, tilt command to tilt moment, and the off-diagonal transfer function, tilt command to yaw moment, for a system of order 10. From this figure, it can be observed that the estimated model, the OpenFAST model, and the spectral average, closely follow the same trend for the diagonal transfer between tilt command and tilt moment, whereas their correspondence is slightly lesser for the off-diagonal transfer possibly due to the coupling.

To further assess the performance of the identified model, 500 seconds of the collected data was excluded from identification and reserved for validation. The validation is performed using a metric known as variance accounted for (VAF), which compares the response of the identified model to input data with the output data from the LES simulation:

$$\text{VAF} = \left(1 - \frac{\text{var}(y - y_{est})}{\text{var}(y)}\right) \cdot 100\%, \tag{5}$$

where var denotes the variance, y is the actual response, and y_{est} is the response from the identified model. The VAF yields a value of 97.7% for both output channels, implying excellent performance. Figure 5 displays the VAFs obtained for the other selected system orders. Orders 6 to 11 are subsequently selected for RGA analysis since they display the highest VAF.

B. Relative gain array

Now that several models have been identified, it is time to quantify the RGA for a range of azimuth offsets. The RGA is computed from the frequency response of the $\text{PBSID}_{\text{opt}}$-identified and OpenFAST model by adding an azimuth offset in the inverse MBC transformation up to 20 degrees. Subsequently, the off-diagonal component is analyzed and the offset with the lowest off-diagonal element, implying the least coupling, is selected as the optimal offset. In Fig. 6, this analysis is displayed, which yields an optimal azimuth offset of 14 degrees for the linearized model obtained from OpenFAST. Interestingly, for all orders 6-11 of the $\text{PBSID}_{\text{opt}}$-identified model, an optimal offset of 17 degrees is found, a consistent 3-degree difference with the azimuth offset obtained from the linearized models in OpenFAST. The required azimuth correction for the phase loss as a result of substepping can be approximated by multiplying the difference in timestep with the rotor speed:

$$(\delta t_2 - \delta t_1)\omega_{\text{r}} \approx \psi_{\text{ss}}, \tag{6}$$

where δt_2 is the timestep of AMR-wind, δt_1 is the timestep of OpenFAST, ω_{r} is the rotational velocity in rad/s, and ψ_{ss} is the azimuth correction required for substepping. In our case, this correction amounts to 1.82 degrees, which only partly explains the 3-degree correction. Further detailed studies should be conducted to fully unravel the composition of the additional azimuth compensation.

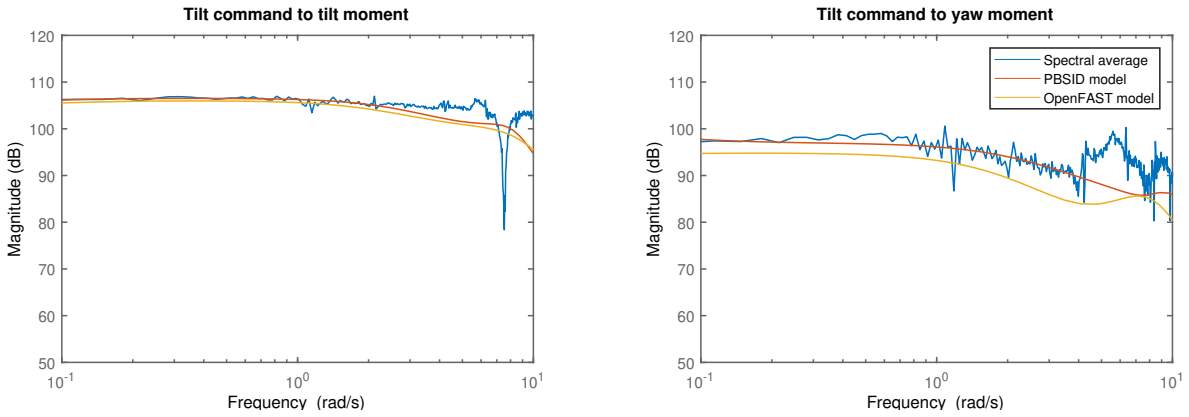

Fig. 4. Bode plots of the spectral average, $\text{PBSID}_{\text{opt}}$-identified model, and OpenFAST linearized model.

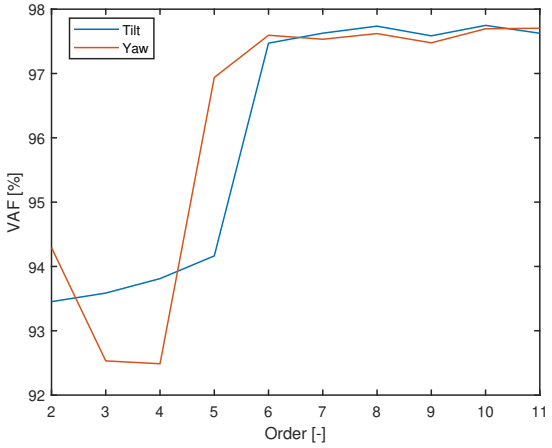

Fig. 5. Comparison of the variance accounted for between each identified model.

C. Sensitivity function

The multivariable sensitivity function is studied here to analyze the effect of the IPC with optimal azimuth offset. In an optimal case, the IPC attenuates the 1P frequency, which is mapped to the DC gain in the fixed frame, while not affecting other frequencies too much. It is further desired that the magnitude difference between the largest and smallest singular value is minimal, such that directionality is reduced. In case of an incorrect azimuth offset, the directionality is large, while for the optimal azimuth offset, it is minimal. The sensitivity function is defined as:

$$S(\mathrm{j}\omega) = (I + L(\mathrm{j}\omega))^{-1}, \tag{7}$$

with $L(\mathrm{j}\omega)$, where ω indicating frequency, denoting the loop transfer defined as:

$$L(s) = P(s)C(s). \tag{8}$$

In the above equation, $P(s)$ is the plant, the $\text{PBSID}_{\text{opt}}$-identified model in our case. In the multivariable case, the control performance is provided by the bounded ratio:

$$\sigma_{\min}(S(\mathrm{j}\omega)) \leq \frac{||y(\omega)||_2}{||v(\omega)||_2} \leq \sigma_{\max}(S(\mathrm{j}\omega)), \tag{9}$$

where $\sigma_{\min}$ and $\sigma_{\max}$ denote the smallest and largest singular value, respectively; $y(\omega)$ and $v(\omega)$ denote the output and measurement signals, respectively.

The multivariable sensitivity function is thus obtained by taking the singular values of the sensitivity functions of the identified system incorporating the azimuth offsets 0, 14, and 17 degrees. Figure 7 shows the largest and smallest singular values, of the three cases. Therein, it can be seen that the system without azimuth offset yields a large magnitude gap between both singular values, including a sensitivity peak above 0 dB for the frequency range between $10^{-1} - 10^{0}$ rad/s, implying an undesired amplification of that region. The 14-degree case is able to remove this sensitivity peak and some of the directionality; however, the 17-degree case displays the smallest difference between the largest and smallest singular value in the sensitivity function from which we derive that it is indeed optimal. Note that the singular values of the optimal azimuth of 17 degrees do not overlap implying directionality is not fully resolved. However, further increasing the offset causes slightly more convergence for low frequencies but divergence for higher frequencies, reaching a less optimal state as confirmed earlier by the RGA.

IV. CONCLUSIONS

In conclusion, this work studied the quantification of the optimal azimuth offset required for individual pitch control. It shed light on the additional phase lags that must be compensated for to justify the use of two SISO control loops for IPC when coupling aeroelastic codes to high-fidelity flow solvers. To tackle this challenge, the authors propose the approach of exciting the structure using PRBN directly in coupled simulations and quantifying the azimuth offset by using black box system identification. The offset derived using this framework directly corrects the additional phase lags and ensures full decoupling of the individual pitch control system.

ACKNOWLEDGMENT

This work is part of the Hollandse Kust Noord wind farm innovation program where CrossWind C.V., Shell, Eneco, Grow, and Siemens Gamesa are teaming up; funding for

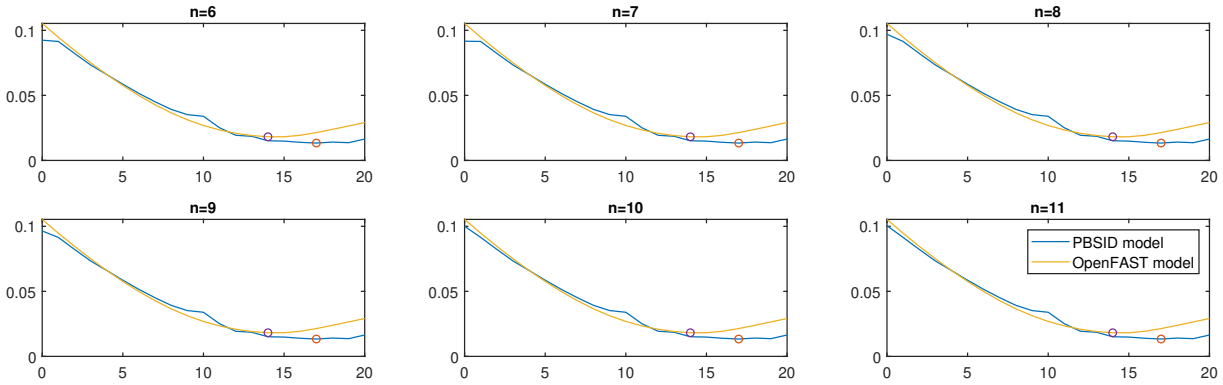

Fig. 6. Comparison of the off-diagonal component of the relative-gain arrays for different azimuth offsets. The optimal offsets are indicated with a circle and n indicates the system order.

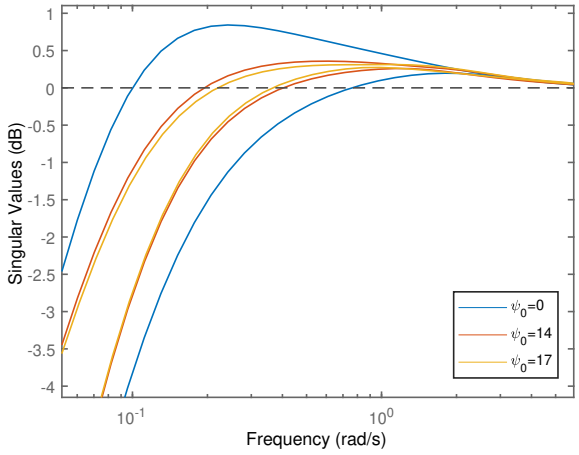

Fig. 7. Multivariable sensitivity function of the PBSID-identified model incorporating different azimuth offsets. The black dashed line indicates the 0dB line, above which the disturbances at these frequencies are amplified and below are attenuated.

the PhDs was provided by CrossWind C.V. and Siemens Gamesa.

References

[1] M. Bilgili and H. Alphan, "Global growth in offshore wind turbine technology," *Clean Technologies and Environmental Policy*, vol. 24, no. 7, pp. 2215–2227, 2022.

[2] T. Burton, N. Jenkins, D. Sharpe, and E. Bossanyi, *Wind energy handbook*. John Wiley & Sons, 2011.

[3] E. A. Bossanyi, "Individual blade pitch control for load reduction," *Wind Energy: An International Journal for Progress and Applications in Wind Power Conversion Technology*, vol. 6, no. 2, pp. 119–128, 2003.

[4] S. P. Mulders, A. K. Pamososuryo, G. E. Disario, and J. W. v. Wingerden, "Analysis and optimal individual pitch control decoupling by inclusion of an azimuth offset in the multiblade coordinate transformation," *Wind Energy*, vol. 22, no. 3, pp. 341–359, 2019.

[5] M. Lara, J. Garrido, J. W. van Wingerden, S. P. Mulders, and F. Vázquez, "Optimization with genetic algorithms of individual pitch control design with and without azimuth offset for wind turbines in the full load region," *IFAC-PapersOnLine*, 2023. 22nd IFAC World Congress.

[6] B. Jonkman, R. M. Mudafort, A. Platt, E. Branlard, M. Sprague, J. Jonkman, H. Ross, M. Hall, G. Vijayakumar, M. Buhl, P. Bortolotti, S. Ananthan, and J. Rood, "OpenFAST/openfast: OpenFAST v3.4.0." Zenodo, Jan. 2023.

[7] M. Brazell, S. Ananthan, G. Vijayakumar, L. Cheung, M. Sprague, E. E. C. P. Team, H. F. M. P. Team, *et al.*, "Amr-wind: adaptive mesh-refinement for atmospheric-boundary-layer wind energy simulations," in *APS Division of Fluid Dynamics Meeting Abstracts*, pp. T29–007, 2021.

[8] L. A. Martínez-Tossas, M. J. Churchfield, and S. Leonardi, "Large eddy simulations of the flow past wind turbines: actuator line and disk modeling," *Wind Energy*, vol. 18, no. 6, pp. 1047–1060, 2015.

[9] N. Troldborg, J. N. Sørensen, and R. Mikkelsen, "Actuator line simulation of wake of wind turbine operating in turbulent inflow," in *Journal of physics: conference series*, vol. 75, p. 012063, IOP Publishing, 2007.

[10] E. Gaertner, J. Rinker, L. Sethuraman, F. Zahle, B. Anderson, G. E. Barter, N. J. Abbas, F. Meng, P. Bortolotti, W. Skrzypinski, *et al.*, "Iea wind tcp task 37: definition of the iea 15-megawatt offshore reference wind turbine," tech. rep., National Renewable Energy Lab.(NREL), Golden, CO (United States), 2020.

[11] W. Zhang, A. Almgren, V. Beckner, J. Bell, J. Blaschke, C. Chan, M. Day, B. Friesen, K. Gott, D. Graves, *et al.*, "Amrex: a framework for block-structured adaptive mesh refinement," *The Journal of Open Source Software*, vol. 4, no. 37, p. 1370, 2019.

[12] N. J. Abbas, D. Zalkind, R. M. Mudafort, G. Hylander, S. Mulders, D. Heff, and P. Bortolotti, "Nrel/rosco: Raaw v1.2," May 2022.

[13] P. Hintjens, *ZeroMQ: messaging for many applications*. " O'Reilly Media, Inc.", 2013.

[14] E. Taschner, A. A. W. van Vondelen, R. Verzijlbergh, and J. W. van Wingerden, "On the performance of the helix wind farm control approach in the conventionally neutral atmospheric boundary layer," in *Journal of Physics: Conference Series*, vol. 2505, p. 012006, IOP Publishing, 2023.

[15] J. N. Sorensen and W. Z. Shen, "Numerical modeling of wind turbine wakes," *J. Fluids Eng.*, vol. 124, no. 2, pp. 393–399, 2002.

[16] J. M. Jonkman and M. L. Buhl, *FAST user's guide*, vol. 365. National Renewable Energy Laboratory Golden, CO, USA, 2005.

[17] S. P. Mulders and J. W. van Wingerden, "On the averaging in the multi-blade coordinate transformations for wind turbines: an h model matching approach," in *2018 IEEE Conference on Control Technology and Applications (CCTA)*, pp. 1631–1637, IEEE, 2018.

[18] A. Chiuso, "The role of vector autoregressive modeling in predictor-based subspace identification," *Automatica*, vol. 43, no. 6, pp. 1034–1048, 2007.

[19] G. Van der Veen, J. W. van Wingerden, M. Bergamasco, M. Lovera, and M. Verhaegen, "Closed-loop subspace identification methods: an overview," *IET Control Theory & Applications*, vol. 7, no. 10, pp. 1339–1358, 2013.

[20] S. Skogestad and I. Postlethwaite, *Multivariable feedback control: analysis and design*. john Wiley & sons, 2005.

[21] M. Verhaegen and V. Verdult, *Filtering and system identification: a least squares approach*. Cambridge university press, 2007.